CHAPTER II

THEORETICAL ASPECTS

The present chapter explains the mechanisms of formation of polyaniline (PAni) nanofibers by dilute polymerization technique. The principle of electrospinning has been discussed with an empahsis on charge generation and separation upon apllication of an electric field. The theories that governed the charge transport in conducting polymers (CPs) have been discussed in brief with the help of current-volatge (I-V) characteristics. The methods for determination of surface energy and its components of the CP based biomaterials' surface have been detailed. In addition, Chapter II includes the theory of Fluorescence Resonance Energy Transfer (FRET) and the description of the method of determination of number of binding sites and binding constants using fluorescence enhancement effect. The theories and equations of enzyme kinetics have been discussed in brief at the end of this chapter.

2.1 Chemical polymerization

Chemical polymerization has been generally accomplished in various solutions, which is one of the most extensively used techniques for large scale synthesis of various conducting polymers (CPs). A solution of soluble precursor can be deposited, when the pH, concentration, and temperature of a solution, at which the precursors are soluble, are changed to a state of supersaturation, crystal nucleation and growth occur [266]. Nucleation and growth of a material occur either in a homogeneous solution or heterogeneously on the surfaces of other solid phases. For successful biomimetic synthesis, heterogeneous nucleation is to be promoted and homogeneous nucleation is to be suppressed. Hence, it is important to understand the various factors that control crystal nucleation and growth in aqueous solutions.

2.1.1 Thermodynamics of nucleation and growth of a material

The supersaturation $\Delta\mu$ (in Joules) is the major driving force for nucleation and growth of a material in solutions is the supersaturation, which is given by [266-268],

$$\Delta\mu = \mu_l - \mu_p \quad (2.1)$$

where μ_l and μ_p are the chemical potentials of a molecule in the solution (l) and in the bulk of the solid phase (p), respectively.

A solution is supersaturated, when $\Delta\mu > 0$, leading to nucleation and/or growth of the precursors. The solution is saturated and undersaturated, when $\Delta\mu = 0$ and $\Delta\mu < 0$, respectively [268].

Using known thermodynamic expressions for μ_l and μ_p, $\Delta\mu$ can be expressed as:

$$\Delta\mu = kTlnS \quad (2.2)$$

where k is the Boltzmann constant, T is the absolute temperature, and S is the degree of supersaturation.

The work required to form a cluster of molecules is defined as the difference between the free energy (ΔG) (in Joules) of the system in its final and initial states, i.e. after and before the cluster formation. However, in reality, the final expression of the work to form a cluster of molecules should contain an additional energy term accounting for the presence of an interface between the cluster and the ambient solution and for the difference of the cluster properties from those of the bulk solid. Thus, taking into account the additional term Φ (in Joules) for effective excess energy of the cluster, the final expression for ΔG can be expressed as below:

$$\Delta G = -\Delta\mu + \Phi \quad (2.3)$$

2.1.1.1 Homogeneous nucleation and growth

When the solution is pure, i.e., only solvent and solute molecules constitute the solution, homogeneous nucleation of the soluble molecules can take place. In homogeneous nucleation, the critical nucleus appears in the centre of the original bulk phase. Nucleation is an activated process and hence, the change in the free energy required for creating the critical nucleus, called as the barrier height, ranges from infinite to zero. Due to such exponential dependence on the barrier height, the rate of the homogeneous nucleation is extremely sensitive to the variation in the temperature, pressure, and intermolecular potentials as well. Therefore, it is necessary to choose the experimental conditions very carefully and the purity of the precursors or the solvent must be ensured. That's why, the occurrence of homogeneous nucleation is very rare to observe outside laboratory conditions.

According to the classical nucleation theory [268], the free energy of forming stable nuclei in the solution can be expressed as:

$$\Delta G_{homo} = -kTlnS + \sigma_{pl} A_{pl} \quad 2.4$$

Where σ_{pl} is the total interfacial energy between the particle (p) and the liquid (l), and A_{pl} is the surface area of the particle in contact with the liquid.

2.1.1.2 Heterogeneous nucleation and growth

Heterogeneous nucleation and growth occur in solutions, which may be constituted of impure molecules and foreign particles including solid substrates that provide active centers for nucleation. The rate of heterogeneous nucleation is much faster than that of homogeneous nucleation rate due to the presence of such impurities. Typically, in one type of heterogeneous nucleation, the nucleus is formed around an impurity molecule or ion or around a tiny impurity, which acts as the nucleation centre of the evolved nucleus [266-268]. In another type, a new phase is formed on planar surfaces of different solid phases e.g., the walls of a container, the surface of suspended particles.

According to the classic theory of nucleation and growth, [268, 269] the free energy of formation of a stable nuclei on a substrate is determined by four parameters, viz. the degree of supersaturation (*S*), the interfacial energy between the particle and the liquid (σ_{pl}), the interfacial energy between the particle and the substrate (σ_{ps}) and the interfacial energy between the substrate and the liquid (σ_{sl}). Thus, according to the classical nucleation theory [268], the free energy of forming stable nuclei on a substrate can be expressed as:

$$\Delta G_{heter} = -kTlnS + \sigma_{pl} A_{pl} + (\sigma_{ps} - \sigma_{sl}) A_{ps} \quad 2.5$$

where A is the surface area of the particle in contact with the liquid (A_{pl}) and the substrate (A_{ps}), k is the Boltzmann constant, and T is the absolute temperature.

2.1.2 Polymerization mechanisms of Polyaniline (PAni)

Synthesis of polyaniline (PAni) and its various nanostructures have been widely carried out by chemical polymerization technique [45, 209, 269]. Electrically conductive PAni is generally synthesized by chemical polymerization of aniline monomers in presence of oxidant and dopant. Ammonium persulfate, $(NH_4)_2S_2O_8$, is generally used as the oxidant for chemical polymerization of PAni due to its because

of its high oxidizing ability. This leads to the incorporation of HSO_4^-/SO_4^{2-} as the dopant anions (A^-) in the product. Besides, other oxidizing agents like $FeCl_3$ etc. have also been employed as the chemical oxidant.

Aniline can be polymerized chemically in acidic environments (pH<3). Generally, aniline is insoluble in water but in acidic medium aniline is converted into anilinium ions that are easily soluble in water. Polymerization in acidic medium restricts the undesired branching in the final product [269]. During chemical polymerization of PAni, the oxidant to monomer ratio is kept at 1:2 primarily because of the fact that $S_2O_8^{2-}$ anion is a two-electron oxidizer (acceptor) and as such during polymerization each aniline monomer loses two electrons.

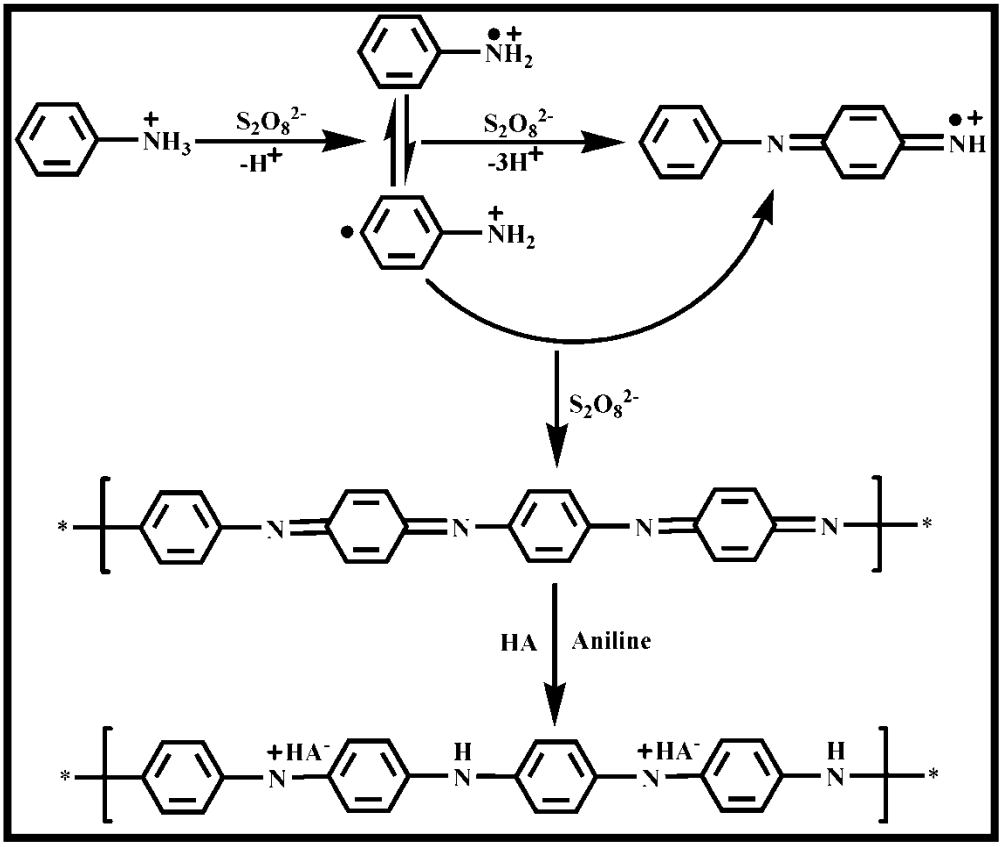

Figure 2.1. Mechanism of chemical polymerization of aniline in presence of oxidant ammonium persulfate, $(NH_4)_2S_2O_8$ as proposed by Epstein *et al* [269].

The proposed mechanism of chemical polymerization of PAni by Epstein *et al.* [269], in presence of oxidant and dopant has been depicted in **Figure 2.1**. During chemical polymerization, aniline molecules are polymerized directly in an oxidant solution (e.g. ammonium persulfate) in the presence of protonic acid such as hydrochloric acid (HCl). Briefly, in the first step, aniline is oxidized to form the anilinium cation-

radical. This step is rate-determining. Two anilinium cation-radical are necessary to form head-to-head, head-to-tail, and tail-to-tail type linkages. In the presence of the strong acids (pH $\leq$ 3), head-to-tail type linkage is in favor of the formation of N-phenyl-1,4-phenylenediamine (aniline dimmer) [269]. N-phenyl-1,4-phenylenediamine is oxidized again to form cation-radical and then reacts with anilinium cation-radical to form trimer. The chain propagates continuously until it terminates when the certain molecular weight is achieved, resulting in the formation of PAni.

2.1.2.1 Dilute polymerization mechanism

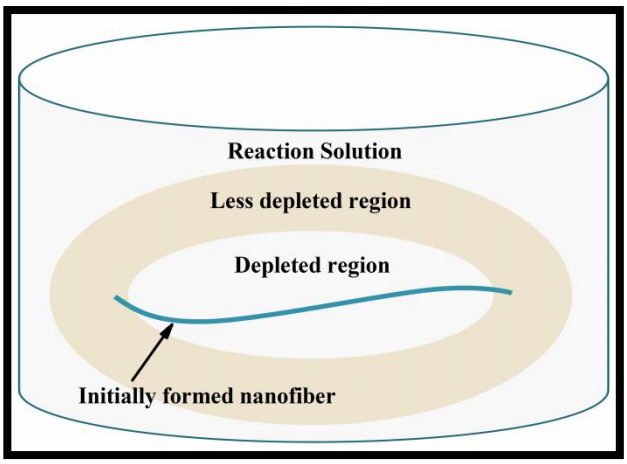

Figure 2.2. Schematic representation of the growth and elongation of an initially formed nanofiber.

According to the classical theory of nucleation and growth, the mechanism of nucleation followed by growth controls the morphology of PAni [266-268]. The formation of PAni in elongated form (e.g., fibers, rods) is established when the growth of PAni is anisotropic in all directions. Furthermore, secondary nucleation causes formation of new active nucleation centers on initially formed nanofibers, resulting in a branched network or dendrites [267]. During dilute polymerization, heterogeneous nucleation involves the formation of the new phase on a (nearly planar e.g., the walls of a container) surface of a different material that are large enough that their surface curvature does not play a role.

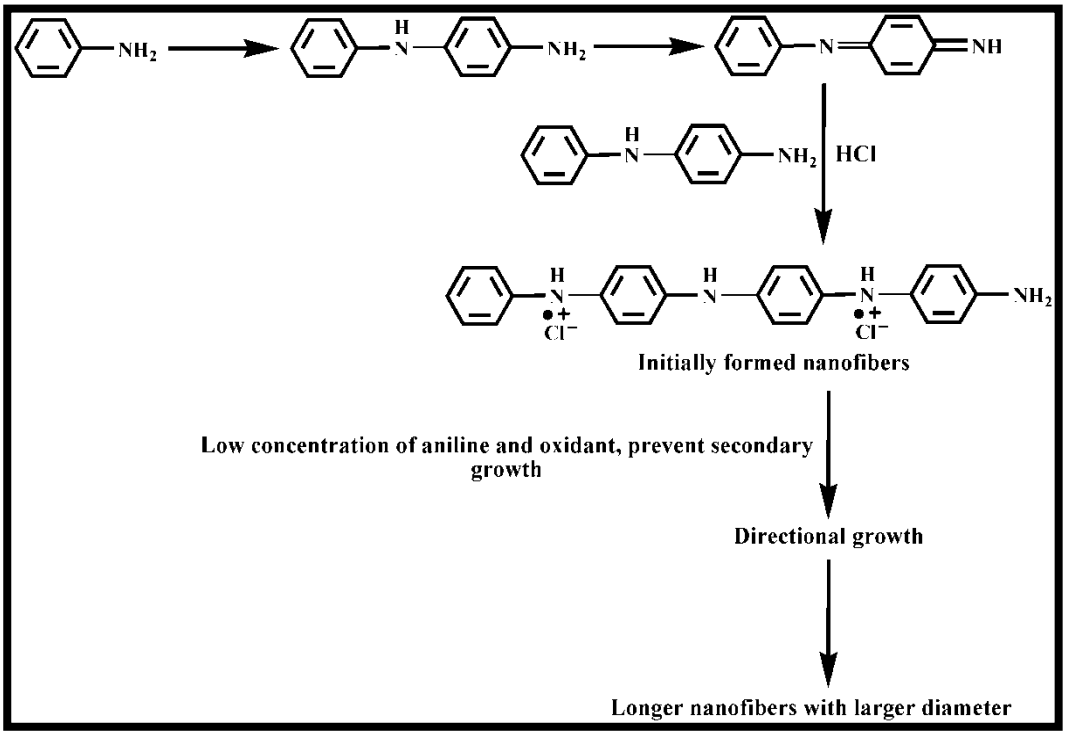

Figure 2.3. Single heterogeneous nucleation mechanism of PAni nanofiber formation according to Chiou *et al* [267].

Generally, during chemical polymerization of PAni, the monomers and oxidants in the vicinity of initially formed nanofibers are depleted in the early stage. Chiou *et al.* [267] proposed that in dilute polymerization, new reactive aniline cation radicals and oligomeric intermediates generally do not diffuse quickly enough to those initially formed nanofibers resulting in nanofibrillar surfaces surrounded by depleted region [**Figure 2.2**]. However, those initially formed nanofibers continuously grow and elongate in one direction because their ends extend to the "less depleted regions" [**Figure 2.2**]. Further, in dilute polymerization, a larger amount of PAni is able to be continuously deposited onto the active nuclei resulting in nanofibers with larger average diameters. This contrasts to the concentrated polymerization in which a large number of nanofibers form suddenly and precipitate, then simultaneously followed by secondary nucleation and growth, resulting in the decrease in the average diameters of the nanofibers [45, 209, 269]. Likewise, PAni begins to grow into highly branched morphology, and then eventually develops into irregular shapes due to secondary nucleation. In contrast, the dilute the monomer/oxidant concentration prevents the secondary nucleation and therefore, the less branched and the longer the nanofibers

with the larger the average diameters are formed in dilute polymerization. Chiou *et al.* further demonstrated that the increased sensitivity to stirring of fiber diameters and lengths for dilute solutions as compared to stirring effects for concentrated solution supports this model of secondary nucleation and the role of depleted regions. Chiou *et al.* showed that thermally activated diffusion kinetics controll the size of the depleted region surrounding each fiber as smaller diameter fibers are produced at lower temperature (e.g., 0^oC as compared to 24^oC synthesis).

Figure 2.3 shows the mechanism of formation of PAni nanofibers by dilute polymerization. Manohar *et al.* first proposed the effect of surface conditions on the formation of PAni nanofibers [270]. As shown in **Figure 2.3**, a fully oxidized aniline dimer can couple with a fully reduced aniline to form aniline tetramer. Oxidation takes place first to the outer surface of a dimer aggregate, as it is in direct contact with the oxidant in solution. Consequently, the reduced or unreacted dimer present in the interior of the aggregate suffers redox coupling and the resultant heat of the reaction introduces fresh aniline dimer for subsequent oxidation.

It is understandable from the proposed mechanism of polymerization of aniline [**Figure 2.1**] that the anilinium cation-radicals are formed in the first step of polymerization. The formation of cations (positive charges) of aniline, dimer, trimer,…,oligomers, etc, as well as emeraldine salt (posses positive charges in the polymer chains) is strongly correlated to anions (the negative charges). Most protonic acids provide anions (A-) in the solution. Anions tend to form ionic bonding (electrostatic force) with cations [267]. Therefore, the aggregation of polymer chains is determined by the electrostatic force, intramolecular forces, and intermolecular forces (e.g. ionic bond, H-bond as well as the van der Waals interactions). The degree of aggregation of polymer chains formed determines the size of nuclei which plays an important role for further growth of nanofibers of PAni. Thus, it can be explained that different dopants can generate different strength of electrostatic force, H-bond, and Van der Waals in the polymerization media and thus, affect the aggregation of oligomeric intermediates or polymer chains resulting in the different sizes of the stable nuclei; hence, producing fibers with different diameters [269].

2.1.2.2 Interfacial polymerization mechanism

Interfacial polymerization is another approach for synthesis of uniform PAni nanofibers without secondary overgrowth as reported by Huang *et al* [45, 209]. This

technique is also based on the principle of chemical oxidative polymerization of aniline monomer in presence of strong acid.

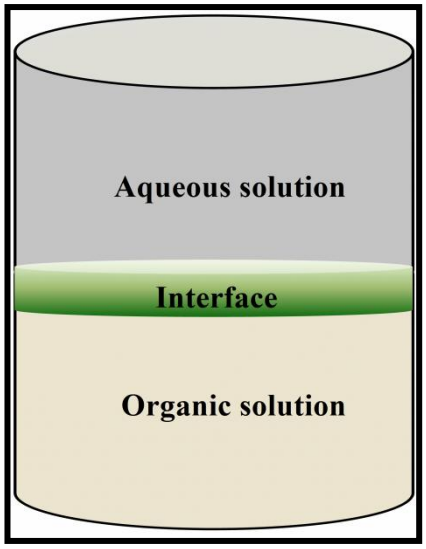

Figure 2.4. Schematic illustration of interfacial polymerization process in a aqueous/organic biphasic solution. The top layer is an aqueous solution consisting of dopant and oxidant, whereas the bottom layer is monomer solution in organic solvent.

Typically, aniline monomer can be dissolved in variety organic solvents such as benzene, hexane, toluene, carbon tetrachloride, chloroform, methylene chloride, diethyl ether, carbon disulfide, or *o*-dichlorobenzene, while the oxidant ammonium peroxydisulfate and dopant (hydrochloric or perchloric acid) is dissolved in water. For interfacial polymerization, both the aqueous and organic solutions are mixed together, which results in the formation of an interface as shown in **Figure 2.4**. The polymerization of aniline takes place at this interface and after polymerization, the polymer (PAni) migrates to the aqueous solution. As the polymer leaves the interface, the polymerization stops and this ultimately diminishes the chance of further nucleation or secondary overgrowth, which is common in the conventional polymerization of aniline resulting mostly granular shaped particles of PAni. Huang *et. al.* suggested that during interfacial polymerization, the formation mechanism of PAni nanofibers is related to the oxidative chemical polymerization process itself and the linear PAni chains.

2.2 Theory of electrospinning

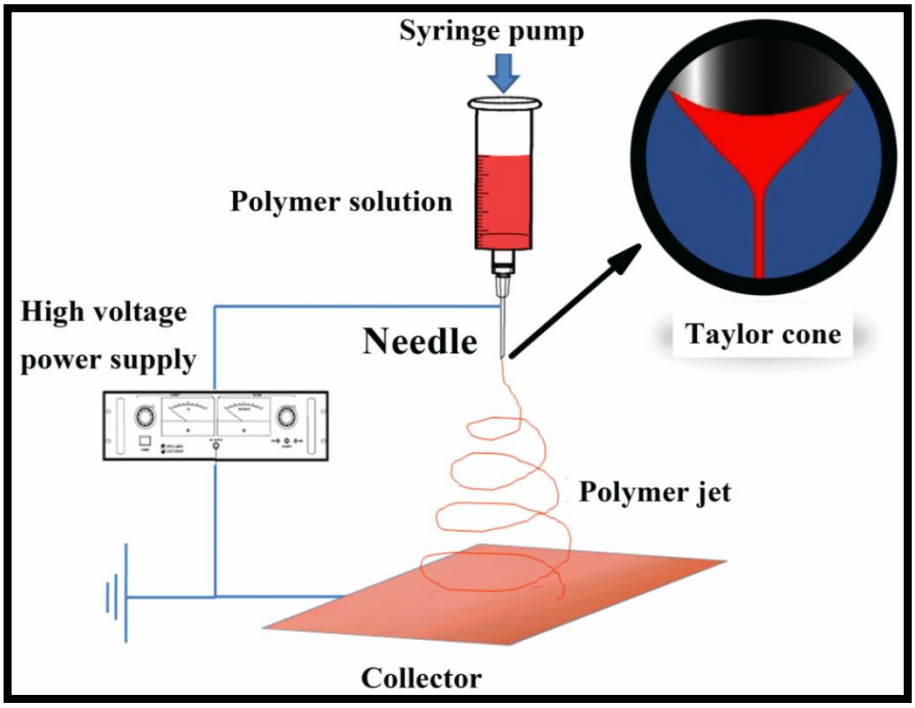

Figure 2.5. Schematic representation of electrospinning process to produce o nanofibers from a polymer solution using syringe and high voltage power supply showing the formation of Taylor cone and subsequent generation of polymer jet deposited on the collector.

Electrospinning is an electrostatic technique where a high electric potential is applied to charge a polymer solution droplet held at the end of a capillary and for subsequent ejection of solution in the form of jet towards the collector. The three necessary components to realize this are as a capillary tube ending in a needle of small diameter, a high voltage power supply, and a grounded metallic collector as shown in **Figure 2.5** [271]. Briefly, the electric filed being applied on the droplet of the polymer solution held by its surface tension at the end of a capillary, induces an electric charge on it. At a critical value of the applied field, the repulsive electrical forces exceed the surface tension and eventually results in the ejection of a charged jet from the tip of the Taylor cone [**Figure 2.5**]. This single charged jet is divided into large number of filaments due to radial repulsion of charges leading to the formation of ultra thin fibers on the grounded collector after evaporation of solvent. The morphology of these ultra thin fibers are highly influenced by the molecular weight, molecular-

weight distribution and architecture of the polymer along with the properties of the electrospinning solution such as viscosity, dielectric constant, surface tension, concentration and other electrospinning parameter such as applied electric field, tip to collector distance, flow rate, collector's size and motion.

2.2.1 Charge generation and transport in polymer solution

The essential first step in electrospinning is the generation of charged polymer solution/melt which can respond to the applied electric field. The generated charges due to the application of an electric field are also subjected to motion as a result of the electrostatic forces being applied. The motion of charge carriers in response to the applied electric field gives rise to electrohydrodynamic phenomena [271, 272]. The electrohydrodynamic phenomenon due to such electrostatic attractions of these excess charges results electrospinning. Charge carriers can be created in a liquid by high electric field induced emission processes at the metal/needle capillary-liquid boundary [272]. This process refers to the direct injection of charges into liquids by emission processes occurring near the electrode. Practically, the charge carriers are always ions, because electrons are easily attached to neutral liquid molecules and cannot exist in a free state [273]. The term "field emission" refers to the process of ejection (often termed "injection") of electrons into the surrounding medium from the surface of an electrode under the influence of a locally high electric field at the metal-liquid boundary. Under these circumstances, electrons can associate with solvent molecules and become ionic current carriers. Similarly, ion emission is the process of ejecting ions into the surrounding fluid as a result of the removal of electrons into the electrode. If the medium were a liquid, these charges simultaneously would produce liquid flow as a result of the electrohydrodynamic effect. The charges in the polymer fluid have a major impact on the Taylor cone formation and the movement of the fiber towards the collecting electrode. However, other characteristics of the charge flow, namely the contribution/discharge of current from the corona surrounding the Taylor cone, charge evaporation, and the dissipation of charge from the fiber after deposition on the collection electrode, are also involved during electrospinning process. While the injected polymer solution allows transport of charges in the liquid phase, the fiber solidifies well before it reaches the substrate. Therefore, any charges that reside in the spun fiber after solidification are trapped either within or on the surface of the fiber.

Figure 2.6 depicts the conceptualization of charge generation, charge transport, charge loss, and residual in the electrospinning process.

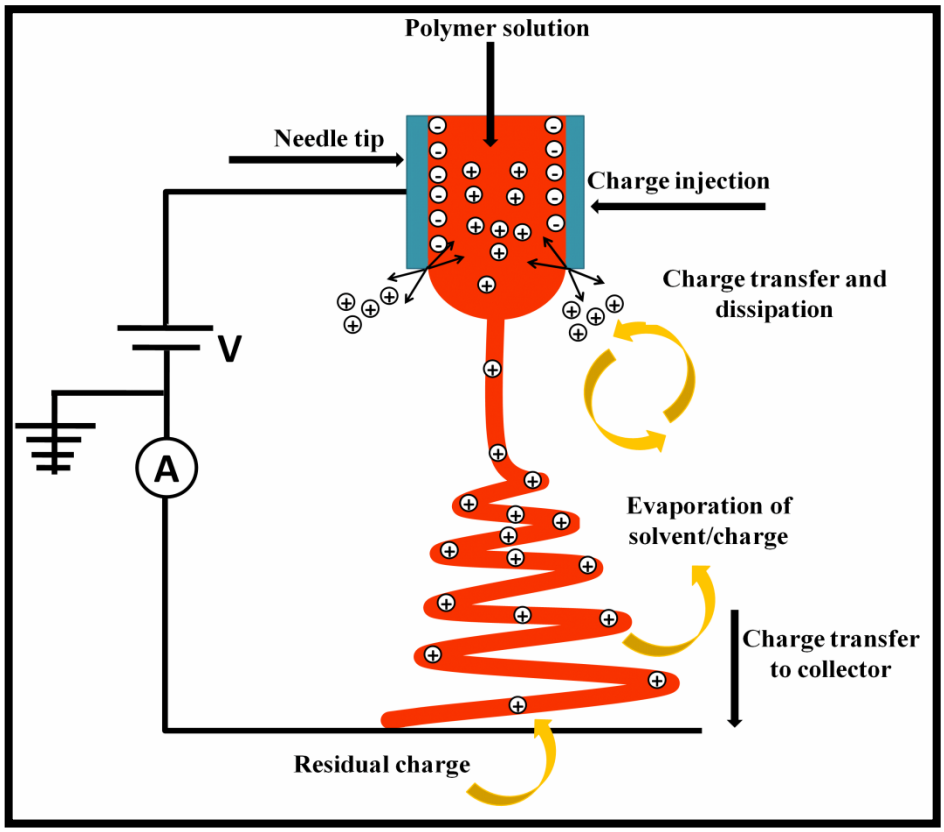

Figure 2.6. Schematic diagram illustrating charge generation and transport during electrospinning.

2.2.2 Droplet generation

The first and foremost step in electrospinning process is the charging of a polymer solution droplet. Usually, a polymer solution is pumped at a low flow rate into a capillary tip. In the absence of an applied electric field, the surface tension of the liquid and the gravitational force, are the only two forces acting on the meniscus of the droplet. Due to the electric field, charge separation takes place as discussed above in a droplet. When the capillary is positively charged, for instance, the positively charged species migrate to the surface of the droplet and the negatively charged species accumulate in its interior until the electric field within the liquid droplet is zero. Charge separation generates a force that is countered by the surface tension within the droplet [274]. The velocity at which these ionic species move through the liquid is determined by the magnitude of the electric field and the ionic mobility of the species.

2.2.3 Taylor cone formation

The deformation of relatively small charged droplets under an electric field, from a sphere to an ellipsoid, has been studied for years [274, 275]. The effect diminishes as radius of the droplet (r) increases, because the electric field just outside the droplet varies inversely with r^2 [274, 275]. For droplets of water, such deformation is observed at fields exceeding 5000V/cm. The elongated droplet assumes a cone-like shape and a narrow jet of liquid is ejected from the capillary [274, 275], as seen in **Figure 2.5**. The Taylor cone is formed at the critical voltage, V_C, applied to a droplet at the end of a capillary of length h and radius R [274, 275] as presented in *Equation 2.6*.

$$V_C^2 = \left(\frac{2L}{h}\right)^2 . \left(ln\left(\frac{2h}{R}\right) - 1.5\right) . (0.117\pi RT) \qquad 2.6$$

Observing the process in a range of different liquids, Taylor determined the equilibrium between surface tension and electrostatic forces to be achieved when the half angle of the cone was 49.38°. This value can, however, be different for different polymer solutions and melts.

2.2.4 Launching of the jet

The coulombic repulsions present in the droplet are usually not sufficient to launch the polymer jet due to the abundant entanglement of polymer chains in concentrated solution. Nevertheless, the surface area has to be increased to accommodate the charge accumulation on the jet surface, and this occurs through the formation of fibers. A slim fibril emanates from the cone to create additional surface area needed to accommodate surface charges, and it initially travels directly towards the grounded collector as shown in **Figure 2.5**.

2.2.5 Elongation of straight segment

When the applied voltage exceeds the critical voltage (V_C), the jet initiation occurs. The coulombic repulsion of surface charges on the jet has an axial component that elongates the jet in its passage towards the collector [274, 276]. Studies revealed that the velocity of the jet as well as the variance in jet velocity increase with distance from the Taylor cone [276]. As a result, the jet diameter decreases rapidly due to both extension and evaporation of the solvent. The initially straight jet reduces in diameter

as it accelerates towards the collector, and the tapering is pronounced in the region below the Taylor cone.

2.2.6 Whipping instability region

The originally straight jet segment regularly becomes unstable and displays bending, undulating movements during its passage towards the collector. The type of instability obtained is dependent on the electric field, with stronger fields favoring whipping instability. The polymer jet undergoes into a series of loops of increasing diameter, spiraling down towards the collector [277]. During whipping instability, the rate of increase in surface area and the solvent evaporation rate are high, which reduces the jet diameter.

2.2.7 Solidification into nanofiber

One of the key factors that control the fiber diameter is solvent volatility [274]. With a solvent of high vapor pressure, the elongation viscosity of the jet may reach levels too high to achieve any further deformation quite early in the whipping instability stage, yielding thick nanofibers. With appropriate selection of solvents and process parameters, extremely fine nanofibers can be electrospun. The nanofibers obtained under the best electrospinning conditions are generally of circular cross-section, continuous, and bead free.

2.3 Current-voltage (*I*-*V*) characteristics

The two-fold coordination in conjugated systems in CPs make these materials susceptible to structural distortion. When doped, the most dominant excitations viz., solitons, polarons and bipolarons are inherently coupled to the chain distortions [278]. As a result, charge transport in disordered polymers is regarded as a hopping mechanism between the localized states that consist of conjugated polymer chain segments [278]. Thus, the theories explaining non-intrinsic charge transport mechanisms in CPs are dominated by thermally activated hopping (or tunneling processes) in which the charge carriers viz., solitons, polarons or bipolarons hop across (or tunnel through) barriers created by the presence of isolated states or domains [278]. The current-voltage (*I*-*V*) characteristics in CPs primarily depend on the carrier density at room temperature, while at low temperature and high electric field, the electric field dependence becomes prominent. Different macroscopic models

have been used to explain the current-voltage (*I-V*) characteristics of CPs in different applied voltage range and are discussed below.

2.3.1 Ohmic conduction

In organic semiconductors, when the injected carrier density is lower than that of thermally generated carriers, the Ohmic conduction is observed. During Ohmic conduction, current *(I)* varies linearly with the applied voltage *(V)* and the relation between current density *(J)* and applied voltage *(V)* is expressed as:

$$J = \frac{e\mu n_c}{d} V \qquad 2.7$$

where *e* is the charge of the carrier, μ is the mobility of the carrier, n_c is the density of the carriers and *d* is the thickness of the sample.

2.3.2 Space charge limited conduction (SCLC)

Space charge limited conduction (SCLC) occurs in low mobility solids, when the concentration of injected carriers exceeds the concentration of intrinsic charge carriers [279]. In this case, the injected carriers produce a space charge region near the electrode material interface, which is responsible for the space charge limited conduction. These charges may be localized or mobile, but create a localized non-uniform electric field and the motion of the charges under the influence of this electric field is known as SCLC, which is a normal phenomenon in organic semiconductors. In the absence of any trapping effects, Mott and Gurney proposed an approximation theory of SCLC according to which the current varies as square of the applied voltage and is expressed as:

$$J = \frac{9}{8} \varepsilon_o \varepsilon_r \mu \frac{V^2}{d^3} \qquad 2.8$$

where ε_0 is the permittivity of free space and ε_r is the relative permittivity of the material. This equation is known as Mott-Gurney law and is applicable in trap-free solids. This behaviour is also observed when all the traps are occupied with charges or when the concentrations of traps are less than that of free carrier concentration [280].

2.3.3 Non-linear I-V characteristics: Kaiser Equation

Low dimensional materials of conducting polymers especially nanotubes and nanowires possess unusual electronic transport properties due to the inhomogeneity present in their structure. These polymers exhibit special structural features, i.e., in some regions, the polymer chains are ordered and in other regions, the chains are disordered. This complex structure in disordered materials including doped polymer and inorganic nanofibers is generally considered as conduction regions or long conducting pathways separated by small insulating barriers. Therefore, in such a quasi-one-dimensional inhomogeneous system, non-linear *I-V* characteristics have been observed because of the non-linearity present in their structure. The FIT conduction mechanism proposed by Sheng [281], characterizes electron transfer across insulating barriers, which can be directly influenced by the voltage fluctuations in the conducting pathways. The mean current density through a barrier when a field E_a is applied across it is evaluated as [282]

$$j(E_a) = \int_{-\infty}^{\infty} dE_T \, j(E_a + E_T) P(E_T) \qquad 2.9$$

where $P(E_T)$ is the probability that the fluctuation field across the junction has the value E_T (which may be in either direction). The tunnelling current $j(E)$ for a total field $E_b = (E_a + E_T)$ in the barrier is denoted as [281]

$$j(E_b) = \frac{me}{8\pi^2 \hbar^3} \int_{-\infty}^{\infty} d\varepsilon \, D(\varepsilon, E_b) \boldsymbol{\Theta} \, (\varepsilon, E_b) \qquad 2.10$$

where m and ε are the carrier mass and energy, respectively. $D(\varepsilon, E_b)$ is the barrier transmission factor approximated by the usual exponential WKB expression with $D(\varepsilon, E_b) = 1$ for energies ε greater than that of the tunnelling barrier, and $\boldsymbol{\Theta}$ (ε, E_b) is the appropriate "supply function" determined by the Fermi factors on each side of the barrier. In terms of structure features of quasi one-dimensional disorder materials and the FIT model, Kaiser et al. proposed a generic expression on the basis of the current fluctuation-assisted tunneling through conduction barriers and thermal activation over the barriers, which can give a good description to the non-linear I-V characteristics in quasi one dimensional system [283]:

$$G = \frac{I}{V} = \frac{G_0\, exp(^{V}/_{V_0})}{1 + [h\, exp(^{V}/_{V_0}) - 1]} \qquad 2.11$$

The meaning of the parameters is as follows: G_0 is the temperature-dependent low-field conductance (the Ohmic term as V tends to zero). The parameter V_0 (which strongly depends on barrier energy) is the voltage scale factor that gives an exponential increase in conductance as V increases. When the field increases such that the difference in Fermi levels on either side of the barriers is comparable to the barrier energy, the conductance of a material will saturate at a value G_h which reflects the larger conductance in the absence of barriers. The parameter $h = {}^{G_0}/_{G_h}$ (where $h < 1$) yields a decrease in the value of G below the exponential increase at higher voltages V.

2.4 Determination of binding sites and binding constant (K_A): Fluorescence resonance energy transfer (FRET)

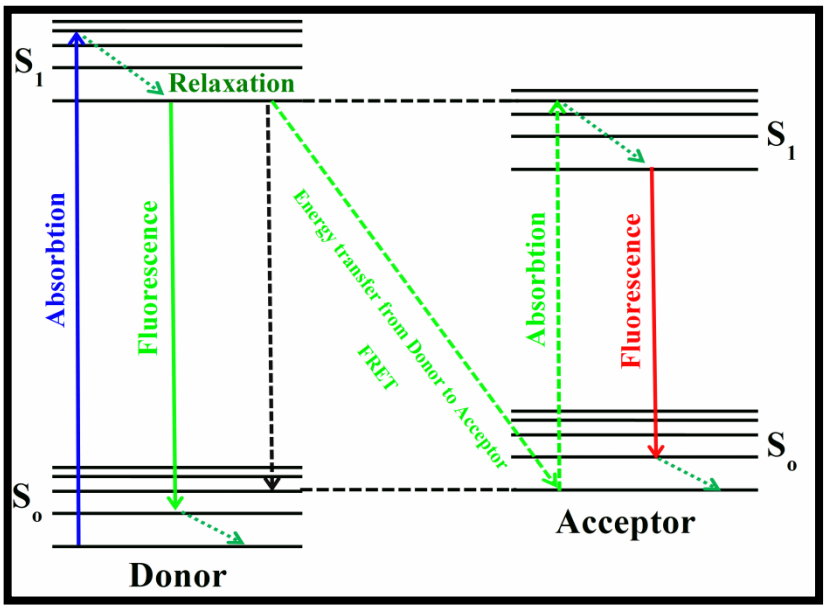

Figure 2.7. Jablonski diagram illustrating the FRET process.

The fluorescence resonance energy transfer (FRET) between two molecules is an important physical phenomenon with considerable interest for the understanding of some biological systems and with potential applications in optoelectronic and thin film device development [284-286]. The technique of FRET, when applied to optical

microscopy, permits to determine the approach between two molecules within several nanometers.

The mechanism of fluorescence resonance energy transfer involves a donor fluorophore in an excited electronic state, which may transfer its excitation energy to a nearby acceptor chromophore in a non-radiative fashion through long-range dipole-dipole interactions. The theory supporting energy transfer is based on the concept of treating an excited fluorophore as an oscillating dipole that can undergo an energy exchange with a second dipole having a similar resonance frequency. In this regard, resonance energy transfer is analogous to the behavior of coupled oscillators, such as a pair of tuning forks vibrating at the same frequency. In contrast, radiative energy transfer requires emission and reabsorption of a photon and depends on the physical dimensions and optical properties of the specimen, as well as the geometry of the container and the wavefront pathways. Unlike radiative mechanisms, resonance energy transfer can yield a significant amount of structural information concerning the donor-acceptor pair.

Resonance energy transfer is not sensitive to the surrounding solvent shell of a fluorophore, and thus, produces molecular information unique to that revealed by solvent-dependent events, such as fluorescence quenching, excited-state reactions, solvent relaxation, or anisotropic measurements. The major solvent impact on fluorophores involved in resonance energy transfer is the effect on spectral properties of the donor and acceptor. Non-radiative energy transfer occurs over much longer distances than short-range solvent effects and the dielectric nature of constituents (solvent and host macromolecule) positioned between the involved fluorophores has very little influence on the efficacy of resonance energy transfer, which depends primarily on the distance between the donor and acceptor fluorophore.

A pair of molecules that interact in such a manner that FRET occurs is often referred to as a donor-acceptor pair. The phenomenon of FRET is not mediated by photon emission. Also it does not even require that the acceptor chromophore to be fluorescent. Although in most of the applications the donor and the acceptor are fluorescent.

In the process of FRET, initially a donor fluorophore absorbs the energy due to the excitation of incident light and transfer the excitation energy to a nearby chromophore, the acceptor.

$$D + h\upsilon \rightarrow D^*$$

$$D^* + A \rightarrow D + A^*$$

$$A^* \rightarrow A + h\upsilon'$$

Here, D and A denote donor and acceptor, respectively.

Energy transfer manifests itself through decrease or quenching of the donor fluorescence and a reduction of excited state lifetime accompanied also by an increase in acceptor fluorescence intensity. **Figure 2.7** is a Jablonski diagram that illustrates the coupled transitions involved between the donor emission and acceptor absorbance in FRET. In presence of suitable acceptor, the donor fluorophore can transfer its excited state energy directly to the acceptor without emitting a photon.

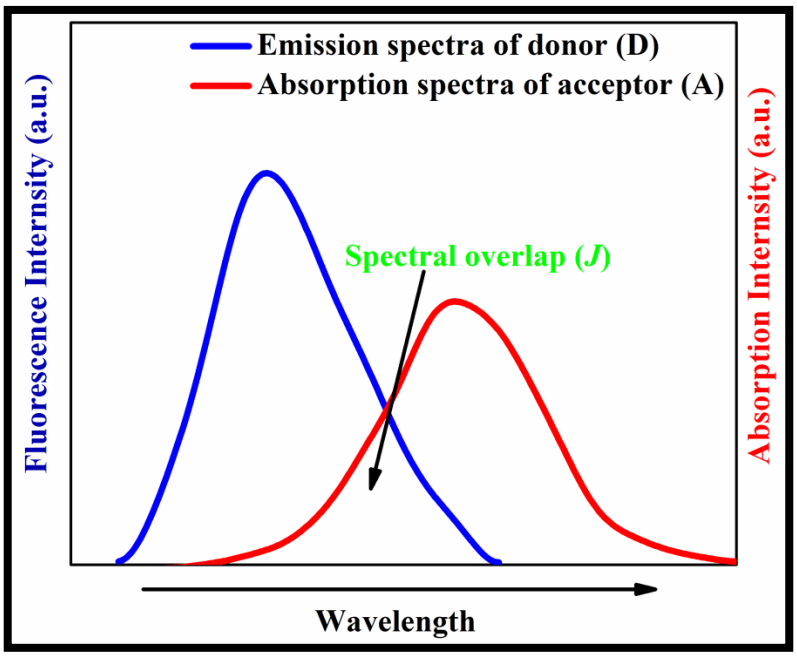

Figure 2.8. Absorption and fluorescence spectra of an ideal donor-acceptor pair showing the spectral overlap between the fluorescence spectrum of donor and absorption spectrum of acceptor.

There are few criteria that must be satisfied in order for FRET to occur. These are: (i) the fluorescence emission spectrum of the donor molecule must overlap the absorption or excitation spectrum of the acceptor chromophore. The degree of overlap is referred to as spectral overlap integral (J) [**Figure 2.8**]. (ii) The two fluorophore (donor and acceptor) must be in the close proximity to one another (typically 1 to 10 nanometer). (iii) The transition dipole orientations of the donor and acceptor must be

approximately parallel to each other. (iv) The fluorescence lifetime of the donor molecule must be of sufficient duration to allow the FRET to occur.

Förster showed that the efficiency of the FRET process (E_{FRET}) depends on the inverse sixth power of the distance between the donor and acceptor pair (r) and is given by [287]:

$$E_{FRET} = \frac{R_o^6}{R_o^6 + r^6} \qquad 2.12$$

Where R_o is the Förster radius at which half of the excitation energy of donor is transferred to the acceptor chromophore. Therefore, Förster radius (R_o) is referred to as the dietance at which the efficiency of energy transfer is 50%. The Förster radius (R_o) depends on the fluorescence quantum yield of the donor in the absence of acceptor (f_d), the refractive index of the solution (η) , the dipole angular orientation of each molecule (K_2) and the spectral overlap integral of the donor-acceptor pair (J) and is given by [287],

$$R_o = 9.78 \times 10^3 \, (\eta^{-4}.f_d.J)^{\frac{1}{6}} \, A^o$$

In summary, the rate of FRET depends upon the extent of spectral overlap between the donor acceptor pair [**Figure 2.8**], the quantum yield of the donor, the relative orientation of the donor-acceptor transition dipole moments and the distance separating the donor-acceptor chromophore. Any event or process that affects the distance between the donor-acceptor pair will affect the FRET rate, consequently allowing the phenomenon to be quantified, provided that the artifacts can be controlled or eliminated.

When biomolecules co-exist with some fluorophore or ligand in a solution, the obvious change in fluorescence intensity can be observed, which can be used to study the binding event of biomolecules with the fluorophore [288-292]. The change in fluorescence intensity of the fluorophore in presence of aromatic amino acids, has been utilized to determine the apparent binding constant (K_A) and the number of binding sites (n) of these complexes. A biomolecule (P) binds with a fluorophore or ligand (M) with 'n' number of same and separating binding sites according to the following reaction:

$$P + nM \leftrightarrow M_nP$$

Accordingly we can obtain the fluorescence enhancement *Equations 2.13-2.15* will be as follows:

$$\frac{[M_t]}{[M_b]} = \frac{1}{K_A(n[P_t] - [M_b])} + 1 \qquad 2.13$$

$$M_b = M_t \times \frac{F - F_D - F_A}{F_b - F_A} \qquad 2.14$$

$$\frac{1}{F - F_D - F_A} = \frac{1}{F_b - F_A}\left(1 + \frac{1}{K_A\,(n[P_t] - [M_b])}\right) \qquad 2.15$$

Where $[M_t]$ is the total concentration of the fluorophore, which is fixed throughout the experiment, $[M_b]$ is the concentration of the fluorophore bound to the biomolecule, $[P_t]$ is the total concentration of biomolecule, the concentration of resultant M_nP can be expressed as $[M_n]/n$, and $[M] = [M_t] - [M_b]$, $[P] = [P_t][M_b]/n$; F is the fluorescence intensity of the fluorophore in presence of biomolecule, F_D is the fluorescence intensity of free biomolecule, F_A is the fluorescence intensity of the free fluorophore and F_b is the maximum fluorescence intensity of the fluorophore after the biomolecule is added to it. According to *Equation 2.15*, the double reciprocal curve of $[F - F_D - F_A]^{-1}$ against $n[P_t] - [M_b]^{-1}$ is plotted varying 'n' from 1 to 3. The curve is a straight line and the slope of the best fitted double reciprocal curve gives the apparent dissociation constant ($K_D = 1/K_A$) and the corresponding value of 'n' is the number of binding sites of the fluorophore-biomolecule complex.

2.5 Determination of surface energy and its components: Contact angle measurement

The atoms at the surface of a condensed phase material are in a very different environment as compared to that of interior. The difference arises due to the asymmetrical environment; in the bulk material, each atom is surrounded by other similar atoms and they experience no net force. However, the atoms that are present at the surface experience this at only one side of the interface. In addition to this, the various influencing factors exerted by the environment act only on the outermost atoms and are in general in higher energy state as compared to that of the interior

atoms. The differences in energy between the atoms at the surface and in the bulk of a material manifest themselves as surface tension (or surface free energy), γ. The surface energy of a non-metallic material can be divided in polar component (γ^{AB}) and apolar component (γ^{LW}). Qualitatively, surface tension is a contractile force that acts in any surface trying to minimize the surface area. Measurement of contact angle is considered as the simplest and the most accurate method for characterizing the surface properties of a solid and determining the interaction between a liquid and a solid at the minimum equilibrium distance [293]. Several methods such as Owens, Wendt, Rabel and Kaelble method (OWRK, also known as Fowkes method), acid base (AB or Van Oss-Chaudhury-Good theory) method, Wu method etc. have been employed to calculate the surface energy of a given surface by using contact angle values of different liquids [294, 295].

2.5.1 Owens, Went, Rabel and Kaelble (OWRK) method

Surface energy of a solid surface can be calculated by using contact angles of a substrate with different liquids i.e., polar and apolar. Owens, Wendt, Rabel and Kaelble have developed a method for the estimation of surface energy of a solid surface by using the contact angles of two different liquids. This method resolves the surface energy into different components, which are additive, i.e.,

$$\gamma_i = \gamma_i^d + \gamma_i^p + \gamma_i^h + \gamma_i^i + \gamma_i^{ab} + \dots\dots\dots \qquad 2.16$$

where superscripts *d, p, h, i* and *ab* represent the dispersion force, polar force, hydrogen bonding force, induction force and acid-base force, respectively.

According to this theory, dispersion interactions are connected with London interactions arising from electron-dipole fluctuations. Owen and Wendt considered the entire component except γ_i^d as polar component(γ_i^p) [296]. Therefore, by considering the work of adhesion, the following relation can be established,

$$\gamma_{SL} = \gamma_S + \gamma_L - 2\sqrt{\gamma_S^d \gamma_L^d} - 2\sqrt{\gamma_S^p \gamma_L^p} \qquad 2.17$$

where γ_S is the surface free energy of the solid, γ_L is the surface free energy of the testing liquid and γ_{SL} is the surface free energy of the solid-liquid interface. Moreover, γ_S^d, γ_S^P, γ_L^d and γ_L^p are the dispersive and polar components of surface tension of solid and liquid, respectively.

On the other hand, the well known Young's equation which describes equilibrium at the three phase contact of solid, liquid and gas is given by

$$\gamma_S = \gamma_{SL} + \gamma_L \cos\theta \qquad 2.18$$

where θ is the contact angle made by the testing liquid with the solid surface [296]. Combining *Equation 2.17* with *Equation 2.18*, we get,

$$\sqrt{\gamma_S^d \gamma_L^d} + \sqrt{\gamma_S^p \gamma_L^p} = 0.5\gamma_L(1 + \cos\theta) \qquad 2.19$$

Equation 2.19 is known as OWRK or Fowkes equation by which we can calculate dispersive (γ_S^d) and polar (γ_S^p) parts of surface tension using the contact angle values of one polar and one apolar liquids.

2.5.2 Van Oss-Chaudhury-Good theory (OCG) or Acid-Base (AB) method

According to this theory, the different components of surface tension can be classified in two broad categories i.e.

$$\gamma_i = \gamma_i^{LW} + \gamma_i^{AB} \qquad 2.20$$

where γ_i^{LW} and γ_i^{AB} are the apolar (Lifshitz-van der Waals) and polar (acid-base) components of surface tension, respectively [297]. The polar interactions are mainly governed by the interactions between Lewis-acid and Lewis-base (hydrogen bonding is a type of acid-base interaction). Since, energy of cohesion, $\Delta G = -2\gamma_i$ by definition, therefore for solid *S* and liquid *L* interaction, *Equation 2.20* can be written as

$$\Delta G_{SL} = \Delta G_{SL}^{LW} + \Delta G_{SL}^{AB} \qquad 2.21$$

where, ΔG_{SL}^{LW} is the free energy change due to Lifshitz-van der Waals interaction, and ΔG_{SL}^{AB} is the same due to acid-base interactions [298]. ΔG_{SL}^{LW} can be expressed by the geometric mean (after Fowkes):

$$\Delta G_{SL}^{LW} = -2\sqrt{\gamma_S^{LW} \gamma_L^{LW}} \qquad 2.22$$

While, Van Oss et al. showed that

$$\Delta G_{SL}^{AB} = -2\sqrt{\gamma_S^+ \gamma_L^-} - 2\sqrt{\gamma_S^- \gamma_L^+} \qquad 2.23$$

where γ_i^+ is the acid part and γ_i^- is the basic part of surface tension.

Substituting *Equation 2.22* and *Equation 2.23* into *Equation 2.21*, we get,

$$\Delta G_{SL} = -2\sqrt{\gamma_S^{LW}\,\gamma_L^{LW}} - 2\sqrt{\gamma_S^+\gamma_L^-} - 2\sqrt{\gamma_S^-\gamma_L^+} \qquad 2.24$$

Young's equation (*Equation 2.18*) shows that

$$\gamma_S = \gamma_{SL} + \gamma_L \cos\theta \qquad 2.25$$

On the other hand, the change in free energy due to solid liquid interaction can be given as

$$\Delta G_{SL} = \gamma_{SL} - \gamma_S - \gamma_L \qquad 2.26$$

Combining *Equation 2.25* and *Equation 2.26*,

$$-\Delta G_{SL} = \gamma_L(1 + \cos\theta) \qquad 2.27$$

which is known as Young-Dupre equation. Substituting *Equation 2.27* into *Equation 2.24*,

$$\gamma_L(1 + \cos\theta) = -2\sqrt{\gamma_S^{LW}\,\gamma_L^{LW}} - 2\sqrt{\gamma_S^+\gamma_L^-} - 2\sqrt{\gamma_S^-\gamma_L^+} \qquad 2.28$$

which is known as the Van Oss-Chaudhury-Good (OCG) thermodynamic approach to determine the values of surface free energy components of solids. This equation contains three unknown components of surface tension, i.e., γ_S^{LW}, γ_S^+ and γ_S^-. To determine these values, it is necessary to determine contact angles of three different liquids of known properties (in terms of γ_L^+, γ_L^- and γ_L^{LW}) on the surface of solid of interest. One can then set up three equations with three unknowns which can be solved to obtain the values of γ_S^{LW}, γ_S^+ and γ_S^-. Once the value of γ_S^+ and γ_S^- is obtained, we can calculate γ_i^{AB} by using the following relation:

$$\gamma_i^{AB} = 2\sqrt{\gamma_i^+\gamma_i^-} \qquad 2.29$$

The percentage of polar component can be calculated by using the following equation:

$$Polarity\ (\%) = \frac{\gamma_i^{AB}}{\gamma_i} \times 100 \qquad 2.30$$

2.6 Enzyme kinetics

Enzymes are proteins specialized to catalyze biological reactions. Enzymes are responsible for thousands of metabolic processes that sustain life. Enzymes are the

catalysts of biological systems and are extremely efficient and specific as catalysts. Enzyme interacts with the reactant molecules, which are commonly known as substrate to form enzyme-substrate complex. The enzyme-catalyzed reactions follow the general principle of usual chemical reactions but also exhibit distinct features that is not usually observed in non-enzymatic reactions, i.e., saturation behaviour with substrate. The effect of substrate concentration on the rate of the enzyme-catalyzed reaction is presented in the **Figure 2.9**. The rate of the reaction is nearly proportional to the initial substrate concentration at low concentration of substrate, and the reaction is approximately first order with respect to substrate. But, as the substrate concentration is increased, the rate of the reaction is no longer proportional to the substrate concentration and the reaction is of mixed order. At high substrate concentration, the rate of the reaction becomes independent of the substrate concentration and in this region; the reaction is essentially zero order with respect to the substrate.

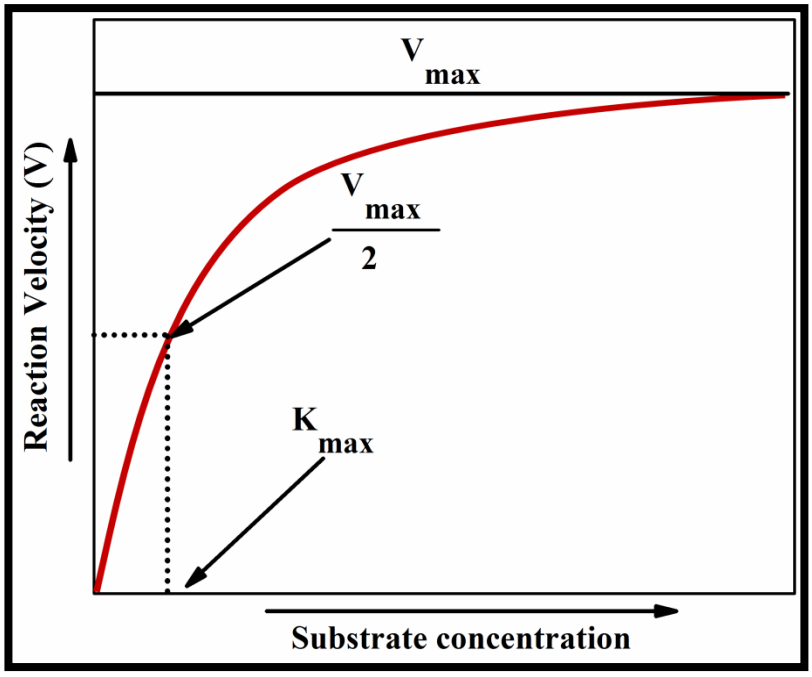

Figure 2.9. The effect of substrate concentration on the rate of an enzyme-catalyzed reaction.

2.6.1 Michaelis-Menten equation

In 1993, L. Michaelis and M. L. Menten developed a general theory of enzyme kinetics, which was further extended by G. E. Briggs and J. B. S. Haldane. The theory is based on the reaction of enzyme with only one substrate. This theory assumes that

the enzyme *E* first combine with the substrate *S* and results in the enzyme-substrate complex (*ES*), which in turn breaks down to form free enzyme and the product *P* [299].

$$E + S \overset{K_{+1}}{\longrightarrow} ES \overset{K_{+2}}{\longrightarrow} E + P \qquad 2.31$$

$$E + S \overset{K_{+1}}{\longleftarrow} ES \overset{K_{+2}}{\longleftarrow} E + P \qquad 2.32$$

These reactions are believed to be reversible and the rate constants for the forward and reverse directions have a positive and negative subscript, respectively. To derive a general expression for V_o, the initial velocity of an enzyme-catalyzed reaction, we have considered the two step reaction mechanism as shown in the *Equation 2.31 and Equation 2.32*. The initial velocity is of course equal to the rate of breakdown of the enzyme-substrate complex *ES*, according to the *Equation 2.31* for which we can write the first order rate equation,

$$V_0 = k_{+2}[ES] \qquad 2.33$$

where $[ES]$ is the concentration of enzyme-substrate complex. However, we cannot determine k_{+2} or $[ES]$ directly. On the other hand, the second order rate equation for the formation of $[ES]$ from *E* and *S* can be written as:

$$\frac{d[ES]}{dt} = k_{+1}([E_T] - [ES])[S] \qquad 2.34$$

where $[E_T]$ is the total enzyme concentration i.e., the sum of free and combined form, $[S]$ represents the substrate concentration and k_{+1} is the second order rate constant. Although ES can be formed from *E* and *P* by reversible reaction, but can be neglected as we are considering the beginning of the reaction in the forward direction, when $[S]$ is very high and $[P]$ is zero or close to zero.

We can write the rate of equation for the breakdown of $[ES]$ by the sum of two reactions; (i) the reaction yielding the product (forward direction) and, (ii) the reaction yielding *E*+*S*. We have then

$$-\frac{d[ES]}{dt} = k_{-1}[ES] + k_{+2}[ES] \qquad 2.35$$

At equilibrium condition, the rate of formation of *ES* is equal to its rate of breakdown, therefore we can write

$$k_{+1}([E_T] - [ES])[S] = k_{-1}[ES] + k_{+2}[ES] \qquad 2.36$$

Rearranging *Equation 2.36*, we obtain

$$\frac{[S]([E_T]-[ES])}{[ES]} = \frac{k_{-1}+k_{+2}}{k_{+1}} = k_M \qquad 2.37$$

The constant k_M is known as Michaelis-Menten constant [].

The equation can then be written as

$$[ES] = \frac{[E_T][S]}{k_M + [S]} \qquad 2.38$$

Using *Equation 2.38*, we can write

$$V_0 = k_{+2}\frac{[E_T][S]}{k_M + [S]} \qquad 2.39$$

When the substrate concentration is so high that essentially all the enzyme in the system is present as the *ES* complex, i.e., when the enzyme is saturated, we reach the maximum initial velocityV_{max} , given by

$$V_0 = \frac{V_{max}\,[S]}{k_M + [S]} \qquad 2.40$$

This equation is known as Michaelis-Menten equation, which established a mathematical relationship between the initial rate of enzyme-catalyzed reaction (V_0), concentration of substrate ([S]) and characteristics of enzyme (K_M). K_M, which is Michaelis constant, is equal to the concentration of the substrate at which the initial reaction velocity is half of the maximum velocity and is independent of the enzyme concentration.

2.6.2 Lineweaver-Burk equation

The Michaelis-Menten relation can be algebraically transformed into other forms which are more useful in plotting experimental data [299]. By taking the reciprocal of both sides of Michaelis-Menten equation, we get

$$\frac{1}{V_o} = \frac{K_M + [S]}{V_{max}\,[S]} \qquad 2.41$$

Rearranging the equation, we have

$$\frac{1}{V_o} = \frac{K_M}{V_{max}\,[S]} + \frac{1}{V_{max}} \qquad 2.42$$

Equation 2.42 is known as the Lineweaver-Burk equation. In this plot, $\frac{1}{V_o}$ is plotted against $\frac{1}{[S]}$ which results in a straight line with slope of $\frac{K_M}{V_{max}}$, an intercept of $\frac{1}{V_{max}}$ on the $\frac{1}{V_o}$ axis, and an intercept of $\frac{-1}{K_M}$ on the $\frac{1}{[S]}$ axis. This type of double reciprocal plot has an advantage of determining more accurate values of V_{max} and K_M.